

Is shrub expansion into grasslands pushed or pulled?

A spatial integral projection model for woody plant encroachment

Trevor Drees^{*a,b}, Brad M. Ochocki^b, Scott L. Collins^c, and Tom E.X. Miller^b

^aDepartment of Biology, Penn State University, State College, PA USA

^bProgram in Ecology and Evolutionary Biology, Department of BioSciences, Rice University, Houston, TX USA

^cDepartment of Biology, University of New Mexico, Albuquerque, NM USA

August 2, 2022

^{*}thd5066@psu.edu

1

Abstract

2 Coming soon.

3

Keywords

4 density-dependence, ecotones, woody encroachment, shrubs, integral projection model,
5 grassland

Introduction

The recent and ongoing encroachment of shrubs and other woody plants into adjacent grasslands has caused significant vegetation changes across arid and semi-arid landscapes worldwide (Cabral et al., 2003; Gibbens et al., 2005; Goslee et al., 2003; Parizek et al., 2002; Roques et al., 2001; Trollope et al., 1989; Van Auken, 2009, 2000). The process of encroachment generally involves increases in the number or density of woody plants in both time and space (Van Auken, 2000), which can drive shifts in plant community structure and alter ecosystem processes (Knapp et al., 2008; Ravi et al., 2009; Schlesinger and Pilmanis, 1998; Schlesinger et al., 1990). Other effects of encroachment include changes in ecosystem services (Kelleway et al., 2017; Reed et al., 2015), declines in biodiversity (Brandt et al., 2013; Ratajczak et al., 2012; Sirami and Monadjem, 2012), and economic losses in areas where the proliferation of shrubs adversely affects grazing land and pastoral production (Mugasi et al., 2000; Oba et al., 2000).

Woody plant encroachment can be studied through the lens of spatial population biology as a wave of individuals that may expand across space and over time (Kot et al., 1996; Neubert and Caswell, 2000; Pan and Lin, 2012; Wang et al., 2002). Theory predicts that the speed of wave expansion depends on two processes: local demography and dispersal of propagules. First, local demographic processes include recruitment, survival, growth, and reproduction, which collectively determine the rate at which newly colonized locations increase in density and produce new propagules. Second, colonization events are driven by the spatial dispersal of propagules, which is commonly summarized as a probability distribution of dispersal distance, or “dispersal kernel”. The speed at which expansion waves move is highly dependent upon the shape of the dispersal kernel, especially long-distance dispersal events in the tail of the distribution (Skarpaas

30 and Shea, 2007). Both demography and dispersal may depend on plant size, since larger
31 plants often have improved demographic performance and release seeds from greater
32 heights, leading to longer dispersal distances (Nathan et al., 2011). Accounting for popu-
33 lation structure, including size structure, may therefore be important for understanding
34 and predicting wave expansion dynamics (Neubert and Caswell, 2000).

35 Theory predicts that the nature of conspecific density dependence is another critical
36 feature of expansion dynamics but this is rarely studied in the context of woody plant
37 encroachment. Expansion waves typically correspond to gradients of conspecific den-
38 sity – high in the back and low at the front – and demographic rates may be sensitive
39 to density due to intraspecific interactions like competition or facilitation. If the demo-
40 graphic effects of density are strictly negative due to competitive effects that increase
41 with density then demographic performance is maximized as density goes to zero, at
42 the leading edge of the wave. Under these conditions, the wave is “pulled” forward by
43 individuals at the low-density vanguard (Kot et al., 1996), and targeting these individ-
44 uals and locations would be the most effective way to slow down or prevent encroach-
45 ment (cite?). However, woody encroachment systems often involve positive feedbacks
46 whereby shrub establishment modifies the environment in ways that facilitate further
47 shrub recruitment. For example, woody plants can modify their micro-climates in ways
48 that elevate nighttime minimum temperatures, promoting conspecific recruitment and
49 survival for freeze-sensitive species (D’Odorico et al., 2010; Huang et al., 2020). Posi-
50 tive density dependence (or Allee effects) causes demographic rates to be maximized at
51 higher densities behind the leading edge, which “push” the expansion forward, leading
52 to qualitatively different expansion dynamics (Keitt et al., 2001; Kot et al., 1996; Lewis
53 and Kareiva, 1993; Sullivan et al., 2017; Taylor and Hastings, 2005; Veit and Lewis, 1996).
54 Pushed expansion waves generally have different shapes (steeper density gradients) and

55 slower speeds than pulled waves (Gandhi et al., 2016), and may require different strate-
56 gies for managing or decelerating expansion (Taylor and Hastings, 2005). The potential
57 for positive feedbacks is well documented in woody encroachment systems as a key fea-
58 ture of bi-stability (the existence of woody and herbaceous habitats as alternative stable
59 states: Wilcox et al. (2018)) but it remains unclear whether and how strongly these feed-
60 backs decelerate shrub expansion and influence strategies for management of woody
61 encroachment.

62 In this study, we linked woody plant encroachment to ecological theory for inva-
63 sion waves, with the goals of understanding how seed dispersal and density-dependent
64 demography drive encroachment, and determining whether the encroachment wave is
65 pushed or pulled. Throughout the aridlands of the southwestern United States, shrub
66 encroachment into grasslands is well documented (D’Odorico et al., 2012) but little is
67 known about the dispersal and demographic processes that govern it. Our work fo-
68 cused on encroachment of creosotebush (*Larrea tridentata*) in the northern Chihuahuan
69 Desert. Expansion of this species into grasslands over the past 150 years has been well
70 documented, leading to decreased cover of *Bouteloua eriopoda*, the dominant foundation
71 species of Chihuahuan desert grassland (Buffington and Herbel, 1965; Gardner, 1951;
72 Gibbens et al., 2005). As in many woody encroachment systems, creosotebush expansion
73 generates ecotones marking a transition from dense shrubland to open grassland, with a
74 transition zone in between where shrubs can often be found interspersed among grasses
75 (Fig. 1).

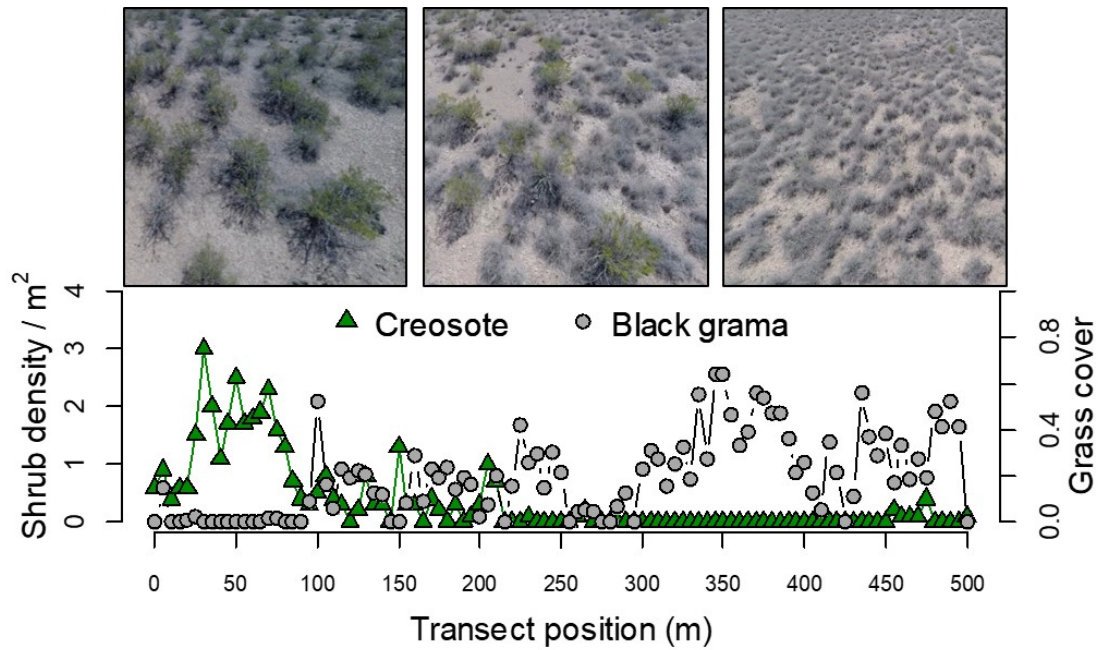


Figure 1: Example of an ecotone transect at Sevilleta LTER, spanning gradients of creosotebush and black grama grass. Photo credits: TEX Miller

76 Historically, creosotebush encroachment into grasslands is believed to have been
 77 driven by a combination of factors including overgrazing, drought, variability in rain-
 78 fall, and suppression of fire regimes Moreno-de las Heras et al. (2016). These shrubs
 79 are also thought to further facilitate their own encroachment through positive feedbacks
 80 (D’Odorico et al., 2012; Grover and Musick, 1990) by modifying their environment in
 81 ways that favor continued growth and recruitment, including changes to the local micro-
 82 climate (D’Odorico et al., 2010) and rates of soil erosion (Turnbull et al., 2010). Such pos-
 83 itive feedback also involve suppression of herbaceous competitors, reducing competition
 84 as well as the amount of flammable biomass used to fuel the fires that keep creosotebush
 85 growth in check (Van Auken, 2000). We hypothesized that, given potential for positive

86 feedback mechanisms, the rarity of conspecifics at the low-density encroachment front
87 may depress demographic performance and generate pushed-wave dynamics.

88 We used a combination of observational and experimental data from shrub ecotones
89 in central New Mexico to parameterize a spatial integral projection model (SIPM) that
90 predicts that speed of encroachment (m/yr) resulting from lower-level demographic and
91 dispersal processes. Our data came from demographic surveys and experimental trans-
92 plants along replicate ecotone transects spanning a gradient of shrub density, and seed
93 drop experiments to estimate the properties of the dispersal kernel. We focused on wind
94 dispersal of seeds, since little is known about the natural history of dispersal in this sys-
95 tem and the seeds lack rewards to attract animal dispersers. We also used re-surveys
96 of permanent transects as an independent measure of encroachment that provided a
97 benchmark against which to evaluate model predictions. The SIPM accounts for size-
98 structured demography of creosotebush, allows us to test whether shrub expansion is
99 pulled by the low-density front or pushed from the high-density core, and identifies the
100 local (demographic) and spatial (seed dispersal) life cycle transitions that most strongly
101 contribute to expansion speed. We address the following specific questions:

- 102 1. What is the nature of conspecific density dependence in demographic vital rates
103 along shrub encroachment ecotones? Is encroachment pulled by the individuals at
104 the front or pushed by individuals behind it?
- 105 2. What is the seed dispersal kernel for this species and how does this vary with
106 maternal plant size?
- 107 3. What is the predicted rate of expansion from the SIPM and which lower-level pro-
108 cesses most strongly affect the expansion speed?
- 109 4. How does the observed rate of encroachment in the recent past compare to model

110 predictions?

111 **Materials and methods**

112 *Study species*

113 Creosotebush *Larrea tridentata* is a perennial, drought-resistant shrub that is native to
114 the arid and semiarid regions of the southwestern United States and northern Mexico.
115 High-density areas of creosotebush consist largely of barren soil between plants due to
116 the “islands of fertility” these shrubs create around themselves (Reynolds et al., 1999;
117 Schlesinger et al., 1996), though lower-density areas will often contain grasses in the
118 inter-shrub spaces (Fig. 1). In our northern Chihuahuan desert study region creosote-
119 bush reproduces sexually, with numerous small yellow flowers giving rise to highly
120 pubescent spherical fruits several millimetres in diameter; these fruits consist of five
121 carpels, each of which contains a single seed. Seeds are dispersed from the parent plant
122 by gravity and wind, with the possibility for seeds to subsequently be transported by
123 animals or water (Maddox and Carlquist, 1985). In other regions, this species also repro-
124 duces asexually and can give rise to long-lived clonal stands (Vasek, 1980), but this does
125 not occur in our study region. The foliage is dark green, resinous, and unpalatable to
126 most grazing and browsing animals (Mabry et al., 1978).

127 *Study site*

128 We conducted our work at the Sevilleta National Wildlife Refuge (SNWR), a Long-Term
129 Ecological Research (SEV-LTER) site in central New Mexico. The refuge exists at the in-
130 tersection of several eco-regions, including the northern Chihuahuan Desert, Great Plains
131 grassland, and steppes of the Colorado Plateau. Annual precipitation is approximately

132 250 mm, with the majority falling during the summer monsoon season from June to
133 September. The recruitment events that facilitate creosotebush expansion are thought
134 to be highly episodic (Peters and Yao, 2012), and this may be linked to fluctuations in
135 monsoon precipitation (Bowers et al., 2004; Boyd and Brum, 1983). Monsoon precipitation
136 during the study years (2013-2017) was [summarise climate data].

137 *Demographic data*

138 *Ecotone transects*

139 We collected demographic data during early June of every year from 2013-2017. This
140 work was conducted at **four sites in the eastern part of SNWR**¹ (one site was initiated
141 in 2013 and the other three in 2014), with three transects at each site. All transects were
142 situated along a shrubland-grassland ecotone so that a full range of shrub densities was
143 captured: each transect spanned core shrub areas, grassland with no or few shrubs,
144 and the transition between them. Lengths of these transects varied from 200 to 600 m,
145 determined by the strength of vegetation transition since “steep” transitions required
146 less length to capture the full range of shrub density.

147 We quantified shrub density in 5-meter “windows” along each transect, including all
148 shrubs within one meter of the transect on either side (shrubs that partially overlapped
149 with the census area were included). Densities were quantified once for each transect
150 (in 2013 or 2014) and were assumed to remain constant for the duration of the study, a
151 reasonable assumption for a species with very low recruitment and very high survival
152 of established plants. Given the population’s size structure, we weighted the density of
153 each window by the sizes of the plants, which we quantified as volume (cm³). Volume
154 was calculated as that of an elliptic cone: $V_i = \frac{\pi h}{3} \frac{lw}{4}$ where l , w , and h are the max-

¹would a map be helpful?

imum length, maximum width, and height, respectively. Maximum length and width were measured so that they were always perpendicular to each other, and height was measured from the base of the woody stem at the soil surface to the tallest part of the shrub. The weighted density for a window was then expressed as $\log(\text{volume})$ summed over all plants in the window.

Observational census

At approximately 50-m intervals along each transect we tagged up to 10 plants for annual demographic census and recorded their local (5-m resolution) window so that we could connect individual demographic performance to local density. These tagged shrubs were revisited every June and censused for survival (alive/dead), size (width, length, and height, as above), flowering status, and fertility of flowering plants (numbers of flower-buds, flowers, and fruits). In instances where shrubs had large numbers of reproductive structures that would be difficult to reliably count (a large shrub may have thousands of flowers or fruits), we made counts on a fraction of the shrub and extrapolated to estimate whole-plant reproduction. Creosotebush does not have one discrete reproductive event per year; instead, flowering may occur throughout much of the warm season. By combining counts of buds, flowers, and fruits we intended to capture a majority of the season's reproductive output, assuming that all buds and flowers will eventually become fruits. Our measurements of reproductive output are therefore conservative and may underestimate total seed production for an entire transition year. Each year, we searched for new recruits within one m on either side of the transect. New recruits were tagged and added to the demographic census. The observational census included a total of 522 unique individuals.

178 *Transplant experiment*

179 We conducted a transplant experiment in 2015 to test how shrub density affects seedling
180 survival. This approach complemented observational estimates of density dependence
181 and filled in gaps for a part of the shrub life cycle that was rarely observed due to low
182 recruitment. Seeds for the experiment were collected from plants in our study popu-
183 lation in 2014. Seeds were germinated on Pro-Mix potting soil (Quakertown, PA) in
184 Fall 2014 and seedlings were transferred to 3.8 cm-by-12.7 cm cylindrical containers and
185 maintained in a greenhouse at Rice University. Seedlings were transported to SNWR
186 and transplanted into the experiment during July 27-31, 2015. Transplant timing was
187 intended to coincide with the monsoon season, when most natural recruitment occurs.

188 The transplant experiment was conducted at the same four sites and three transects
189 per site as the observational demographic census, where we knew weight shrub densities
190 at 5-m window resolution. We established 12 1-m by 1-m plots along each transect. Plots
191 were intentionally placed to capture density variation: four plots were in windows with
192 zero shrubs, four plots were placed in the top four highest-density windows on the
193 transect, and the remaining four plots were randomly distributed among the remaining
194 windows with weighted density greater than zero. Plots were placed in the middle of
195 each 5-m window (at meter 2.5) and were divided into four 0.5-m by 0.5-m subplots.
196 We divided each subplot into nine squares (0.125-m by 0.125-m) and recorded ground
197 cover of each square as one of the following categories: bare ground, creosotebush,
198 black grama (*B. eriopoda*), blue grama (*B. gracilis*), other grass, or “other”. Each subplot
199 received one transplanted shrub seedling, for a total of 48 transplants per transect, 144
200 transplants per site, and 576 transplants in the entire experiment. Each site was set
201 up on a different day and there was a significant monsoon event after the third and
202 before the fourth site. This resulted in differential mortality that appears to be related

203 to site (captured as a statistical random effect) but more likely reflects the timing of the
204 monsoon event relative to planting (moist soil likely promoted transplant survival). We
205 revisited the transplant experiment on October 24, 2015 to survey mortality. After that
206 first visit, transplants were censused along with the naturally occurring plants each June,
207 following the methods described above.

208 *Demographic analysis*

209 We fit statistical models to the demographic data and used AIC-based model selection to
210 evaluate empirical support for alternative candidate models. The top statistical models
211 were then used as the vital rate sub-models of the SIPM, so there is a strong connection
212 between the statistical and population modeling, as is typical of integral projection mod-
213 eling. Our analyses focused on the following demographic vital rates: survival, growth,
214 probability of flowering, fertility (flower and fruit production), seedling recruitment, and
215 seedling size. Most of these vital rates were modeled as a function of plant size, and all
216 of them included the possibility of density dependence.

217 The alternative hypotheses of pushed versus pulled wave expansion rest on how the
218 rate of population increase (λ), derived from the combination of all vital rates, respond
219 to density. We were particularly interested in whether demographic performance was
220 maximized as local density goes to zero (pulled) or at non-zero densities behind the
221 wave front (pushed). To flexibly model density dependence and detect non-monotonic
222 responses, we used generalized additive models in the R package ‘mgcv’ (Wood, 2017).
223 For each vital rate, we fit candidate models with or without a smooth term for local
224 weighted density (among other possible covariates). To avoid over-fitting, we set the
225 ‘gamma’ argument of gam() to 1.8, which increases the complexity penalty, results in
226 smoother fits (Wood, 2017), and makes our approach more conservative (other gamma

values yielded qualitatively similar results). We pooled data across transition years for analysis. All models included the random effect of transect (12 transects across 4 sites); we did not attempt to model both site and transect-within-site random effects due to the low numbers of each. All vital rate functions used the natural logarithm of volume (cm^3) as the size variable and the sum of $\log(\text{volume})$ as the weighted density of a transect window.

Survival. We modeled survival or mortality in year $t + 1$ as a Bernoulli random variable with three candidate models for survival probability. These included smooth terms for initial size in year t only (1), initial size and weighted density (2), and both smooth terms plus an interaction between initial size and weighted density (3). We analyzed survival of experimental transplants and observational census plants together in the same analyses, with a fixed effect of transplant status (yes/no) included in all candidate models. Since recruits and thus mortality events were both very rare in the observational survey, this approach allowed us to “borrow strength” over both data sets to generate a predictive function for size- and possibly density-dependent survival while statistically accounting for differences between experimental and naturally occurring plants. Because we had additional, finer-grained cover data for the transplant experiment that we did not have for the observational census, we conducted an additional stand-alone analysis of transplant survival that explored the influence of shrub and grass density at multiple spatial scales (Appendix).

Growth. We modeled size in year $t + 1$ as a Gaussian random variable. There were nine candidate models for growth. The simplest model (1) defined the mean of size in year $t + 1$ as a smooth function of size in year t and constant variance. Models (2) and (3) had constant variance but the mean included smooth terms for initial size and weighted

251 density (2) or both smooth terms plus an interaction between initial size and weighted
252 density (3). Models 4-6 had the same mean structure as 1-3 but defined the standard
253 deviation of size in year $t + 1$ as a smooth function of initial size. Models 7-9 mirrored 4-6
254 and additionally included a smooth term for weighted density in the standard deviation.
255 Modeling growth correctly is important because it defines the probability of any future
256 size conditional on current size, a critical element of the IPM transition kernel. We
257 verified that the AIC-selected model described the data well by simulating data from it
258 and comparing the moments (mean, variance, skewness, and kurtosis) of simulated and
259 real data.

260 *Flowering and fruit production.* We modeled shrub reproductive status (vegetative or
261 flowering) in year t as a Bernoulli random variable with three candidate models for
262 flowering probability. These included smooth terms for current size (in year t) only (1),
263 size and weighted density (3), and both smooth terms plus an interaction between size
264 and weighted density. We modeled the reproductive output of flowering plants (the sum
265 of flowerbuds, open flowers, and fruits) in year t as a negative binomial random variable.
266 There were three candidate models for mean reproductive output that corresponded to
267 the same three candidates for flowering probability.

268 *Recruitment and recruit size.* We modeled seedling recruitment in each transect window
269 as a binomial random variable given the number of total seeds produced in that window
270 in the preceding year. There were two candidate models, with and without an influence
271 of weighted density on the per-seed recruitment probability. To estimate window-level
272 seed production, we used the best-fit models for flowering and fruit production and
273 applied this to all plants in each window that we observed in our initial density surveys.
274 We assume that recruits come from the previous year's seeds and not from a long-lived

275 soil seed bank.

276 We modeled recruit size as a Gaussian-distributed random variable and fit four can-
277 didate models including an influence of weighted density on mean, variance, both, and
278 neither.

279 *Density-dependent IPM*

280 The size- and density-dependent statistical models comprised the sub-models of a den-
281 sity dependent Integral Projection Model (IPM) that we used to evaluate how the shrub
282 population growth rate responded to con-specific density; we present this non-spatial
283 model before layering on the spatial dynamics generated by seed dispersal. A basic
284 density-independent IPM predicts the number of individuals of size x' at time $t + 1$
285 ($n(x', t + 1)$) based on a demographic projection kernel (K_{dem}) that gives the rates of tran-
286 sition from sizes x to x' from times t to $t + 1$ and is integrated over the size distribution
287 from the minimum (L) to maximum (U) sizes. In a density-dependent IPM, components
288 of the projection kernel may respond to population abundance and structure:

$$289 \quad n(x', t + 1) = \int_L^U K_{dem}(x', x, \tilde{n}(t)) n(x, t) dx \quad (1)$$

290 Here, $\tilde{n}(t)$ is some function of population structure $n(x, t)$ such as the total density of
291 conspecifics ($\tilde{n}(t) = \int n(x, t) dx$) or, as in our case, total density weighted by size ($\tilde{n}(t) =$
292 $\int x n(x, t) dx$). For simplicity, in the analyses that follow we do not model density as
293 a dynamic state variable; instead, we treat density as a static covariate ($\tilde{n}(t) = \tilde{n}$) and
294 evaluate the IPM at a range of density values. As in our statistical modeling, the size
295 variable of the IPM (x, x') was $\log(\text{cm}^3)$.

296 For our model, the size- and density-dependent demographic transitions captured by
297 the projection kernel include growth or shrinkage (g) from size x to x' conditioned on

298 survival (s) at size x (combined growth-survival function $G(x', x, \tilde{n}) = g(x', x, \tilde{n})s(x, \tilde{n})$),
 299 and the production of new size- x' individuals from size- x parents ($Q(x', x, \tilde{n})$). Repro-
 300 duction reflects the probability of flowering at size x (p), the number of seeds produced
 301 by flowering plants (d), the per-seed probability of recruitment (r), and the size distribu-
 302 tion of recruits (c). Collectively, the rate at which x -sized individuals produce x' -sized
 303 individuals at density \tilde{n} is given by the combined reproduction-recruitment function
 304 $Q(x', x, \tilde{n}) = p(x, \tilde{n})d(x, \tilde{n})r(\tilde{n})c(x', \tilde{n})$. Thus, we can express the projection kernel as:

$$305 \quad K_{dem}(x', x, \tilde{n}) = G(x', x, \tilde{n}) + Q(x', x, \tilde{n}) \quad (2)$$

306 For analysis, we evaluated the IPM kernel over a range of local densities from the mini-
 307 mum to the maximum of weighted density values from the 5-meter windows ($0 \leq \tilde{n} \leq$
 308 \tilde{n}_{max}). At each density level, we discretized the IPM kernel into a 200×200 approxim-
 309 ating matrix and calculated the asymptotic growth rate $\lambda(\tilde{n})$ as its leading eigenvalue. We
 310 extended the lower (L) and upper (U) integration limits to avoid unintentional “eviction”
 311 using the floor-and-ceiling method (Williams et al., 2012).

312 We sought to characterize the shape of density dependence: whether fitness declined
 313 monotonically or not with increasing density. We quantified uncertainty in the density-
 314 dependent growth rate $\lambda(\tilde{n})$ by bootstrapping our data. For each bootstrap, we ran-
 315 domly sampled 75% of our demographic data, re-ran the statistical modeling and model
 316 selection, and used the top vital rate models to generate $\lambda(\tilde{n})$ for that data subset. We
 317 repeated this procedure for 500 bootstrap replicates.

Dispersal modelling

WALD dispersal model. Dispersal kernels were calculated using the WALD, or Wald analytical long-distance dispersal, model that uses a mechanistic approach to predict dispersal patterns of plant propagules by wind. The WALD model, which is based in fluid dynamics, can serve as a good approximation of empirically-determined dispersal kernels (Katul et al., 2005; Skarpaas and Shea, 2007) and may be used when direct observations of dispersal are not available. Under the assumptions that wind turbulence is low, wind flow is vertically homogenous, and terminal velocity is achieved immediately upon seed release, the WALD model simplifies a Lagrangian stochastic model to create a dispersal kernel that estimates the likelihood a propagule will travel a given distance (Katul et al., 2005). Our dispersal kernel takes the form of the inverse Gaussian distribution

$$p(r) = \left(\frac{\lambda'}{2\pi r^3} \right)^{\frac{1}{2}} \exp \left[-\frac{\lambda'(r - \mu')^2}{2\mu'^2 r} \right] \quad (3)$$

that is a slight adaptation² from equation 5b in Katul et al. (2005), using r to denote dispersal distance. Here, λ' is the location parameter and μ' is the scale parameter, which depend on environmental and plant-specific properties of the study system. (We use λ' for consistency with notation in related papers, but λ' the dispersal location parameter should not be confused with λ the geometric growth rate.) The location and scale parameters are defined as $\lambda' = (H/\sigma)^2$ and $\mu' = HU/F$; these are functions of the height H of seed release, wind speed U at seed release height, seed terminal velocity F , and the turbulent flow parameter σ that depends on both wind speed and local vegetation roughness. We parameterized the WALD dispersal kernel using windspeed data from the SEV-LTER weather station nearest our study site (Moore and Hall, 2022) and seed

²unclear what this refers to

terminal velocity data from laboratory-based seed-drop experiments (Appendix A). We integrated the dispersal kernel over observed variation in wind speeds, seed terminal velocity, and release height within the height of a shrub. Therefore the dispersal kernel for a shrub of height U was given by:

$$K_{disp} = \iiint p(F)p(U)p(z)p(r) dF dU dz \quad (4)$$

and $p(F)$ and $p(U)$ are the PDFs of the terminal velocity F and wind speed U , respectively, and $p(z)$ is the uniform distribution from the minimum seed release height ($0.15m$, the height at which grass cover interferes with wind dispersal) to H . Methods for our seed data collection and technical details of dispersal kernel modeling are provided in Appendix A.

Spatial integral projection model

We used a spatial integral projection model to piece together seed dispersal and density-dependent demography, and generate predictions for the rate of shrub expansion that results from this combination of local and spatial processes. The spatially explicit model builds upon the non-spatial model (Eq. 1) and adds a spatial variable (z, z') such that demographic transitions occur across both time and space according to a combined demography-dispersal kernel \tilde{K} :

$$n(x', z', t + 1) = \int_{-\infty}^{+\infty} \int_L^U \tilde{K}(x', x, z', z, \tilde{n}(z, t)) n(x, z, t) dx dz \quad (5)$$

Here, $\tilde{K}(x', x, z', z, \tilde{n}(z, t))$ describes the transition from size x and location z to size x' and location z' given density $\tilde{n}(z, t)$ at starting location z . As before, \tilde{n} is a function of population structure – in our model, weighted local density – but here integrated

over an explicit competitive “neighborhood”: $\tilde{n}(z, t) = \int_{z-h}^{z+h} \int_L^U x n(x, z, t) dx dz$ where h represents neighborhood size in the units of z . The demography-dispersal kernel \tilde{K} is given by the sum of two parts, one that describes reproduction coupled with dispersal of propagules, and another that describes growth and survival of non-dispersing individuals:

$$\tilde{K}(x', x, z', z, \tilde{n}(z, t)) = K_{disp}(z' - z)Q(x', x, \tilde{n}) + \delta(z' - z)G(x', x, \tilde{n}) \quad (6)$$

Here, regeneration function Q and growth-survival function G correspond to Eq. 2, dispersal kernel K_{disp} corresponds to Eq. , and the Dirac delta function is a probability distribution with all mass at zero, which prevents movement. Following standard assumptions for integro-difference equations, we assume that space is one-dimensional and homogeneous, such that demographic transitions do not depend on location (or, more precisely, that they depend on location only through spatial variation in density) and the probability of dispersing from location z to z' depends only on the absolute distance between them.

Under many conditions, models of this form generate traveling waves, and we are particularly interested in the velocity (m/yr) of this wave. Methods to estimate this velocity depend strongly on how demography responds to density. If fitness is maximized at some density $\tilde{n} > 0$ then the wave is pushed and wave velocity can only be estimated through numerical simulation. However, if fitness is maximized at $\tilde{n} = 0$ then the wave is pulled and an upper bound on its asymptotic velocity can be calculated analytically, following Neubert and Caswell (2000) and Jongejans et al. (2011), as

$$c^* = \min_{s>0} \left[\frac{1}{s} \ln(\rho_s) \right] \quad (7)$$

where s is a wave shape parameter and ρ_s is the dominant eigenvalue of the kernel $H_s(x', x)$. Corresponding to Eq. 6 and assuming $\tilde{n} = 0$, H_s is composed of

$$H_s(x', x) = M(s, x)Q(x', x) + G(x', x) \quad (8)$$

where $M(s, x)$ is the moment-generating function (MGF) for the dispersal kernel associated with size x . This formulation of the model assumes that the dispersal kernel depends only on maternal size x and not offspring size x' . To estimate $M(s, x)$ we simulated $N = 10000$ dispersal events (r) for each size x and marginalized these over one spatial dimension as in Lewis et al. (2006). We then evaluated the empirical MGF for each size x : $M(s) = \frac{1}{N} \sum_{i=1}^N e^{sr}$.

We used numerical sensitivity analysis to compare the contributions of demography and dispersal processes to the speed of expansion. We perturbed each vital rate function by an arbitrary value, recalculated wavespeed, and quantified sensitivity as the change in wavespeed divided by the perturbation. Analytical sensitivity analysis is also possible (Ellner et al., 2016) but these sensitivities reflect infinitesimally small perturbations. We were particularly interested in the effects of large perturbations, especially large changes in seedling recruitment, which is subject to pulse events.

Estimates of wavespeed and its sensitivity to demography and dispersal processes were bootstrapped for a total of 1000 replicates. Each bootstrap replicate recreated size- and density-dependent demographic models using 50% resampling on the original demographic data, and recreated dispersal kernels also using 50% resampling on the wind speeds and seed terminal velocities. Model selection for demographic vital rates was run for each bootstrap replicate. The empirical MGF relied on numerical sampling and was therefore sensitive to extreme long-distance events that differed across bootstrap realizations. Therefore, bootstrapped distributions reflect the combination of model un-

407 certainty, parameter uncertainty, and stochasticity inherent to empirical MGFs.

408 *Encroachment re-surveys*

409 Finally, we used re-survey data from permanent transects to assess the predictions of
410 the SIPM with respect to independent empirical observations. In summer 2001, shrub
411 percent cover was recorded along two permanent 1000-m transects that spanned the
412 shrub-grass ecotone (these were different transects than those described above for shrub
413 demography). Surveys were conducted again in summer 2013 to document change in cre-
414 osotebush abundance and spatial extent. At every 10 meters, shrub cover was recorded
415 in nine cover classes (<1%, 1–4%, 5–10%, 10–25%, 25–33%, 33–50%, 50–75%, 75–95%,
416 >95%). For visualization, we show midpoint values of these cover classes at each meter
417 location for both transects and years.

418 **Results**

419 *Size and density dependent demography*

420 Demographic data from naturally occurring and transplanted individuals revealed strong
421 size- and density-dependence in demographic vital rates. For most sizes and vital rates,
422 shrub density had negative demographic effects; there was no strong evidence for posi-
423 tive density dependence in any demographic process at any size. Statistical support for
424 size- and density-dependence is provided in Tables B1–??, which provide AIC rankings
425 for candidate models based on the complete data set.

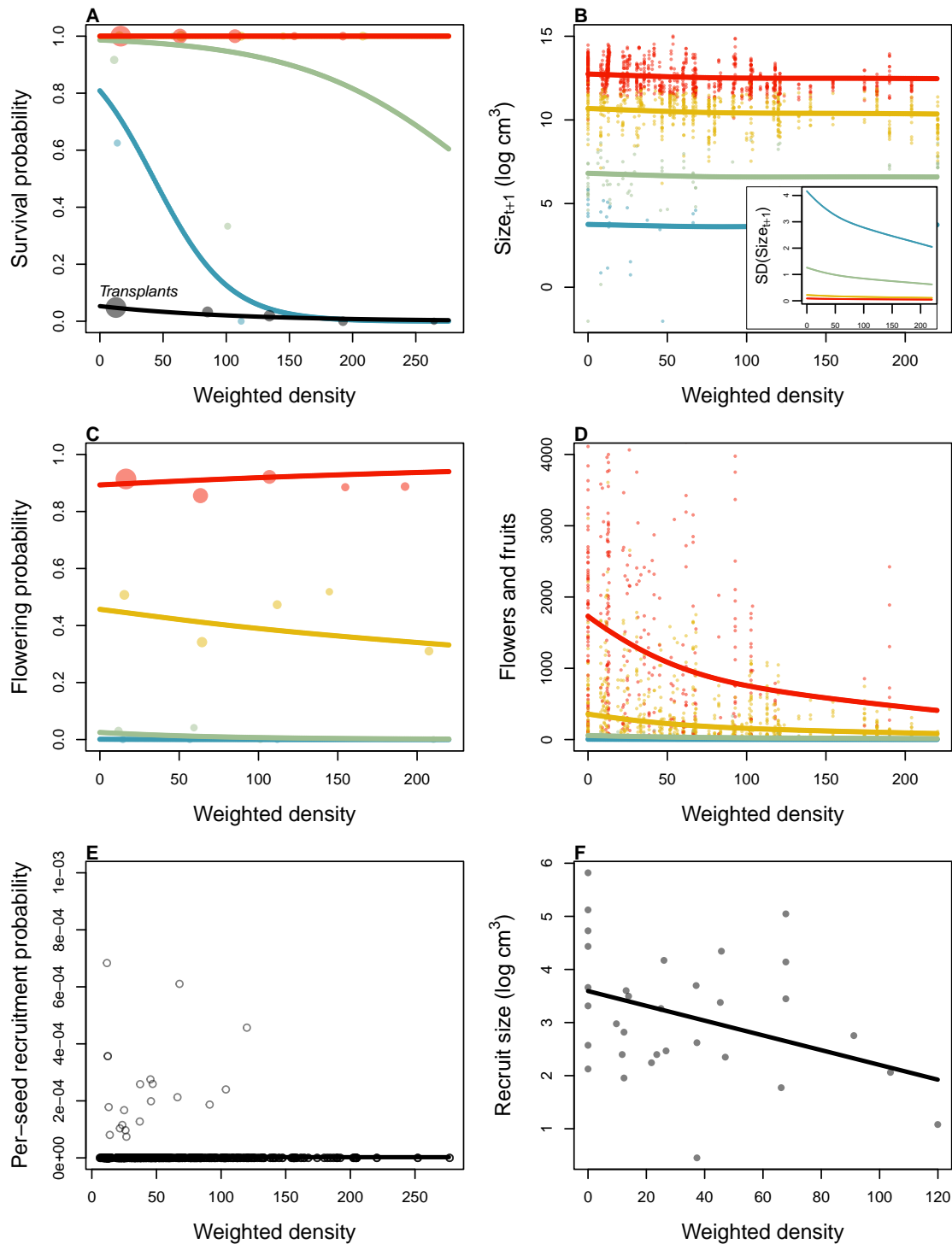


Figure 2: Size- and density-dependence in demographic vital rates. **A** Probability of survival from natural population census and transplant experiment (black line), **B** Mean and variance (inset) of size conditional on previous size, **C** Probability of flowering, **D** Flower and fruit production, **E** Probability of recruitment per seed, **F** Recruit size. In **A**–**E**, colored lines indicate four size groups (red is largest, blue is smallest), discretized for data visualization only. In all panels, weighted density is the sum of all plant sizes $\log(\text{cm}^3)$ within the same 5-m window as the census individual.

426 *Survival.* Among naturally occurring plants, survival of large, established individuals
427 was very high (Fig. 2A). We observed relatively few mortality events and nearly all of
428 these were among new recruits. The probability of survival at these small sizes declined
429 with increasing density. Survival of transplants was very low, lower even than survival
430 of similarly-sized, naturally occurring recruits (Fig. 2B). However, the transplant results
431 support the general pattern of negative density dependence in survival. Among the
432 20 survivors, 15 of them occurred in transect windows below the median of weighted
433 shrub density. In Appendix XX, we show that transplant mortality was dominated by
434 negative effects of shrub density at the 5-m window scale, even when effects of local grass
435 and shrub cover were included as alternative or additional statistical covariates, which
436 suggests that this is the appropriate spatial scale for modeling density dependence in
437 this system.

438 *Growth.* Current size was strongly predictive of future size, as expected, and there was
439 weak negative density dependence in mean future size conditioned on current size (Fig.
440 2C). However, there was a stronger signal of density dependence in the variance of fu-
441 ture size (Fig. 2C, inset). Plants at low density exhibited greater variance in growth
442 trajectories and this was especially true at the smallest sizes. Thus, large increases (and
443 decreases) in the size of new recruits were most likely to occur under low-density condi-
444 tions.

445 *Flowering and fruit production.* Flowering probability was strongly size-dependent and
446 and very weakly sensitive to local density (Fig. 2D). However, fertility of flowering plants
447 was strongly negative density dependent, with greatest flower and fruit production by
448 the largest plants at the lowest densities, and vice versa (Fig. 2E).

449 *Recruitment and recruit size.* We observed 32 natural recruitment events along our tran-
450 sects during the study years and our estimate recruitment rate, given total expected seed
451 production in each window preceding the recruitment year, was very low (2.47×10^{-6} ,
452 2E). While most recruitment events occurred at low density, this is also where most seed
453 production was concentrated (Fig. 2E) and low-density windows were over-represented
454 relative to high density. For these reasons we were more likely to observe recruitment
455 events at low density. Controlling for sampling effort and seed production, the sta-
456 tistical models indicated that our data were most consistent with a constant, density-
457 independent recruitment rate (Table XX). However, the mean size of new recruits de-
458 clined significantly with local density (Fig. 2F).

459 *Population growth rate.* As expected given the vital rate results, the asymptotic popula-
460 tion growth rate λ declined monotonically with density (Fig. 3). This was true across
461 nearly all bootstrap replicates, indicating high certainty that shrub fitness is maximized at
462 zero density and thus that the expansion wave is “pulled” (for this reason our wavespeed
463 results are based on the analytical approach described above). Mean growth rate at low
464 density was 3% per year, with bootstrap uncertainty spanning 1–6%. At high density in
465 the core of the expansion wave, population growth rates approached $\lambda = 1$, indicating
466 population stasis driven by near-perfect survival and extremely rare recruitment.

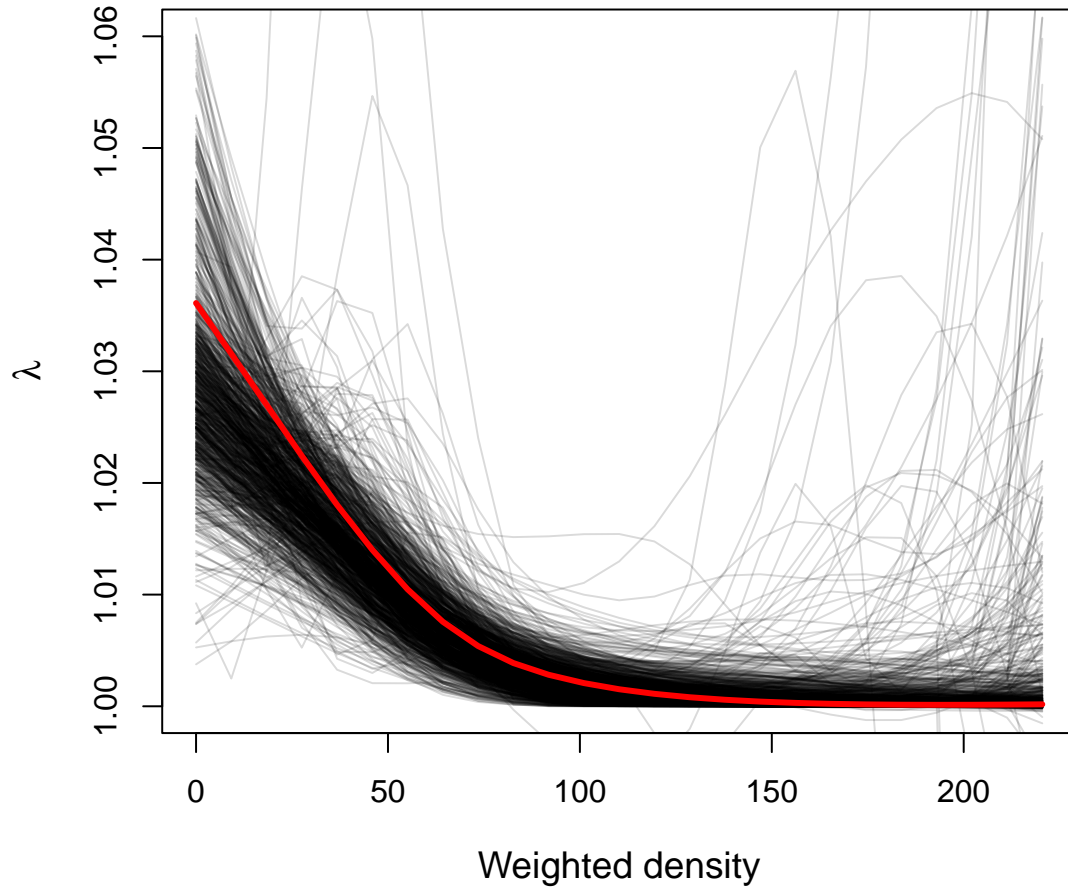


Figure 3: Density dependence in the asymptotic population growth rate (λ). Lines show bootstrap replicates sub-sampled from the full demographic data set. Weighted deighted density is the sum of all plant sizes $\log(\text{cm}^3)$ within 5-m windows.

Seed dispersal

467

468 WALD dispersal kernels, inferred from the properties of seeds and wind and account-
 469 ing for observed variation in wind speeds and within-plant seed release height, were
 470 predicted to be strongly size dependent, with taller plants having a greater probability

471 of dispersing seeds longer distances (Fig. 4). However, predicted seed dispersal was
472 highly local, with most seeds expected to fall within one meter of parent plants for most
473 sizes. Even for the very tallest shrub we observed (1.96 m), only 6.2% of its seeds were
474 predicted to fall more than 3 m away and less than 1% were predicted to fall more than
475 6 m away (Fig. 4). Taller shrubs also exhibited wider variance in their dispersal kernel
476 and this reflects their wider range of seed release heights.

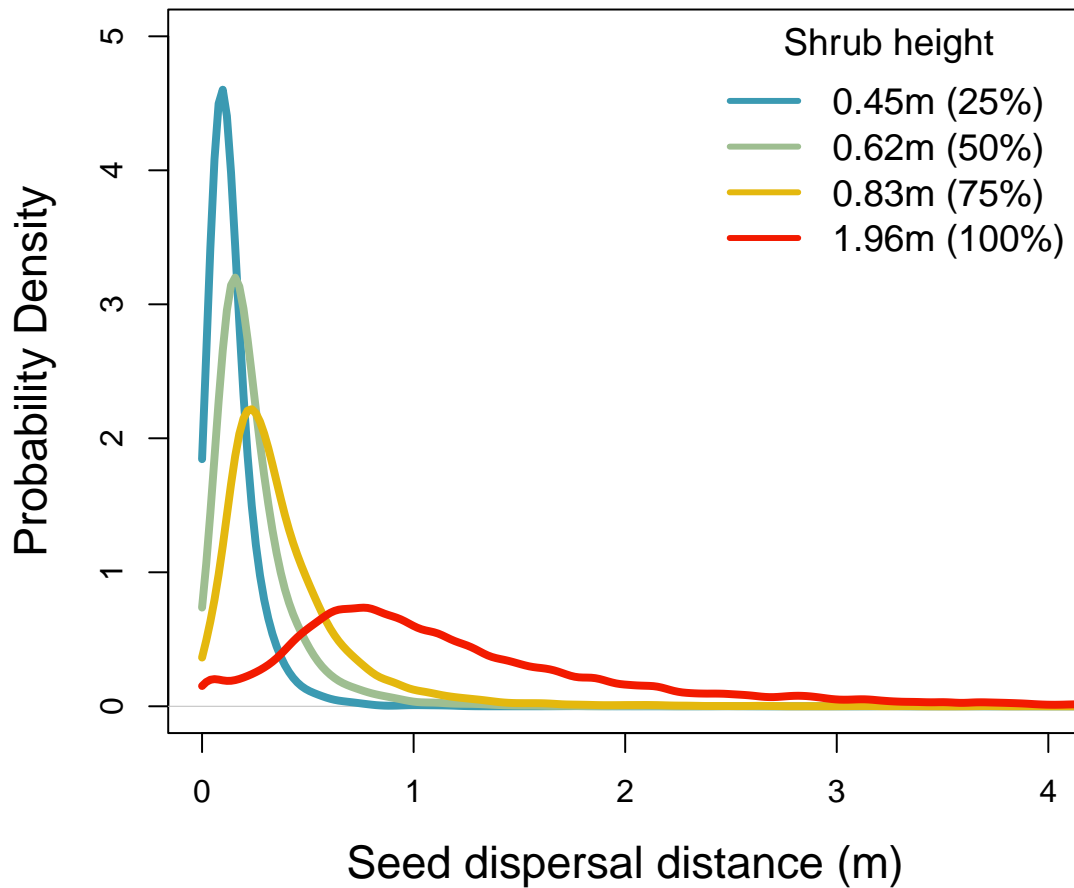


Figure 4: Predicted WALD dispersal kernels for four shrub heights corresponding to the 25th, 50th, 75th, and 100th (maximum) percentiles of the observed size distribution. We assume that heights below 15 cm have effectively no seed movement due to interference with the grass layer.

Expansion speed and sensitivities

477

478 The asymptotic speed of creosote encroachment, given the above demography and dis-
 479 persal patterns, was very slow. The mean asymptotic speed was VALUE m/year and
 480 the 5–95 percentiles of the uncertainty distribution was VALUE m/year (Fig. 6A). Ex-

481 pansion speed was by far the most sensitive to the probability of seedling recruitment
482 (Fig. 6B), indicating that this life cycle transition is imposes the strongest constraint on
483 encroachment. Sensitivity to survival ranked second, and since nearly all mortality oc-
484 curred at the smallest sizes this too can be interpreted as an early life cycle constraint on
485 expansion.

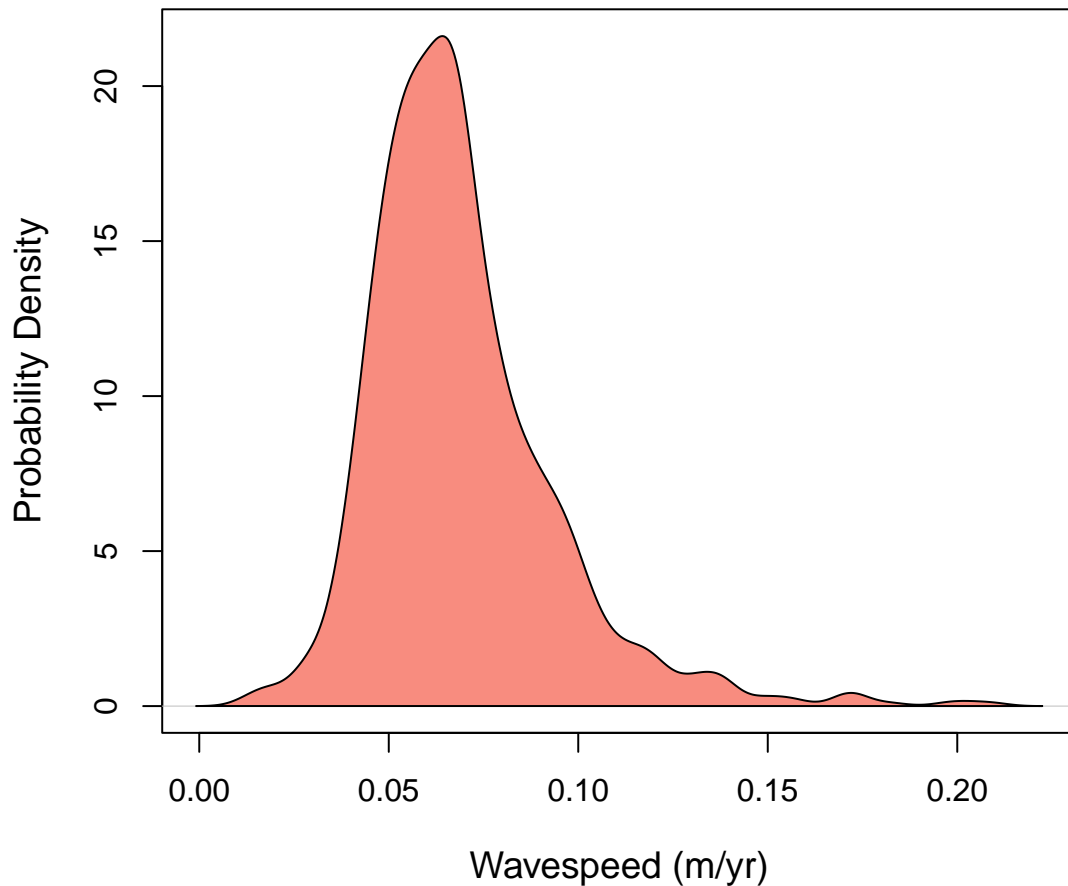


Figure 5: Estimated encroachment wave speeds (left) and geometric rates of population growth (right) for higher post-rainfall seedling survival and normal conditions.

486

Transect re-surveys

487 Re-surveys along two permanent transects revealed virtually no change the in the cre-
 488 osote expansion wave over the 12 years that preceded our study. There were local
 489 changes in percent cover: on average cover increased by XX% between surveys. How-
 490 ever, there was no clear indication that the leading edge of the creosote shrubland has
 491 advanced (the modest right-ward shift on both transects is within the range of measure-
 492 ment error).

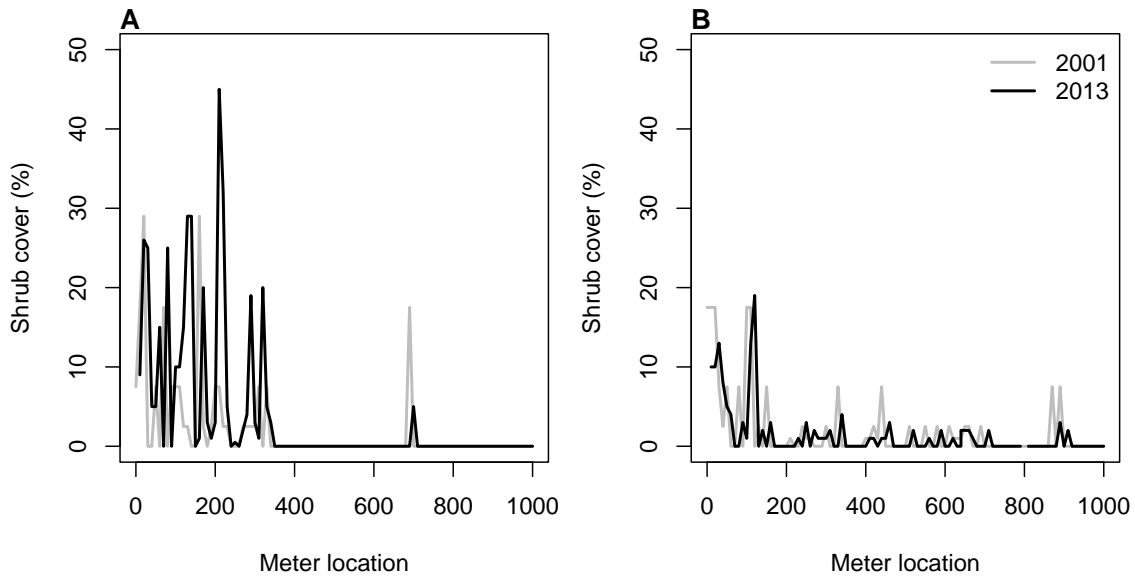


Figure 6: Surveys of creosotebush percent cover along two permanent transects (A,B) in 2001 and 2013.

493

Discussion

494 The encroachment of grasslands by woody plants is a worldwide phenomenon with
 495 broad implications for biodiversity and ecosystem function. To our knowledge, ours is

the first study to apply spatial population biology theory to woody plant encroachment. This perspective on the problem brings attention to the combined influence of dispersal and density-dependent demography as critical controls on the occurrence and pace of encroachment. Through this lens, we asked whether the encroachment process is pushed or pulled, hypothesizing that potential for positive feedbacks may cause declines in fitness at the low-density front and generate pushed-wave dynamics. Instead, observational and experimental evidence indicate that fitness was maximized in low-density plant neighborhoods. The creosote encroachment wave is therefore predicted to be pulled by maximum demographic performance at the leading edge. However, our field-parameterized spatial integral projection model revealed that this wave is pulled at the very slow rate of 5–10 centimeters per year – so slow that, under the observed conditions, this grass-shrub ecotone is effectively stationary. In fact, to our knowledge, ours is the slowest wavespeed estimate for a plant population in the demography-dispersal modeling literature (SIPMs and their matrix model progenitor: (Neubert and Caswell, 2000)). Re-surveys of permanent transects independently supported this prediction, showing virtually no change in the position of the shrub boundary in over a decade. Whatever historical conditions allowed for shrub encroachment to its current extent, the encroachment wave is presently stalled. Below, we discuss and interpret these key findings and their broader implications in greater detail.

Observational and experimental evidence strongly indicated that effects of shrub density were strongly negative in all vital rates and at all sizes. This was surprising given widespread evidence for positive feedbacks (which should generate low-density fitness penalties) in woody plant encroachment generally (D’odorico et al., 2013) and specifically in our creosote bush system (D’Odorico et al., 2010). How can we square these apparently conflicting results? First, it may be important to consider the distinction be-

521 tween “demographic” and “component” Allee effects (Stephens et al., 1999), which refer
522 to effects that manifest in total fitness and components of fitness, respectively. That is,
523 positive effects of conspecific density may occur but in our measures of demographic
524 performance these are swamped by stronger, counter-acting negative effects. It is worth
525 noting that our demographic measurements are temporally coarse, reflecting aggregate
526 performance over a full transition year. More mechanistic studies on finer time scales
527 might reveal component Allee effects that are masked by strong net-negative density
528 dependence. Second, many of the potential mechanisms for positive feedbacks at shrub-
529 grass ecotones would manifest infrequently. For example, effects of shrub encroachment
530 on microclimate (D’odorico et al., 2013) may promote shrub survival only in the face of
531 rare climate events such as extreme low temperatures. Similarly, positive feedbacks that
532 occur via fire suppression (Collins et al., 2021; Ratajczak et al., 2011) would only manifest
533 on timescales that are inclusive of fire return intervals. These considerations suggest that
534 we may be more likely to detect positive density dependence over longer time scales
535 that encompass conditions that trigger positive feedbacks. This leads to the hypothesis
536 that the shrub encroachment wave is *usually* pulled but occasionally pushed. To our
537 knowledge such switches have never been empirically documented in any expanding
538 population but may be an important feature of expansion in fluctuating environments.

539 The very low transplant survival and recruitment rates that we measured also call
540 attention to time scale. Previous studies suggest that creosote recruitment is strongly
541 episodic, likely in response to large, infrequent monsoon precipitation events (Allen
542 et al., 2008; Boyd and Brum, 1983; Moreno-de las Heras et al., 2016). Similar patterns
543 of episodic recruitment driven by large precipitation events have been observed in other
544 cases of woody plant encroachment in aridlands (Harrington, 1991; Weber-Grullon et al.,
545 2022). With only four transition-years of demographic data, we chose to combine infor-

mation across years and build a deterministic model that averages over inter-annual variability. The connection between shrub recruitment and monsoon precipitation, combined with the observed and projected increase in the variability of monsoon precipitation in our study region (Petrie et al., 2014), suggest that extending our deterministic model to accommodate inter-annual variability in climate and climate-dependent vital rates will be a critical next step. Because our wavespeed estimate is acutely sensitive to the seed-to-seedling transition, more so than any other demographic or dispersal process, we expect that a stochastic model incorporating many years of data may yield a faster predicted expansion speed driven by rare pulses of recruitment (Ellner and Schreiber, 2012). Such pulses have clearly not occurred during our study years (2013–2017) or the preceding decade of transect re-surveys (2001–2012) and therefore we think the deterministic model is an adequate representation of the observed conditions. However, our findings of pulled-wave dynamics and strong wavespeed sensitivity to seedling recruitment indicate that the present shrub ecotone is primed for expansion once the necessary climate conditions align, as they likely will in a more variable climate regime. While monsoon precipitation is a leading candidate for factors promoting seedling establishment, it is worth noting that our study years included both the lowest and second-highest amounts of monsoon precipitation in a 20-year record, and yet these events did not correlate with seedling recruitment on our transects (Fig. ??).

While not as strong a constraint as recruitment based on our sensitivity analysis, limited dispersal ability also contributed to the very slow predicted speed of encroachment. Our mechanistic dispersal modeling assumes that wind is the sole dispersal vector. Previous work suggests that this modeling approach can accurately predict dispersal patterns for wind-dispersed plants (Skarpaas and Shea, 2007), yet in our system it may be important to consider secondary dispersal vectors. Boyd and Brum’s 1983 study of cre-

571 osote bush reproductive biology described “contradiction in the literature about mode
572 of dispersal”, citing evidence for a dominant role of wind but the additional possibil-
573 ity of seed movement by granivorous animals. Combining wind and animal dispersal
574 vectors into a “total” dispersal kernel (Rogers et al., 2019) may be a valuable next step.
575 Second, overland flow of runoff may contribute to secondary seed movement following
576 initial deposition by wind (Thompson et al., 2014). Interestingly, seed movement from
577 overland flow would be most likely following large monsoon events. Therefore the same
578 conditions that promote seedling recruitment may also promote long-distance dispersal,
579 potentially amplifying a pulse of shrub encroachment (Ellner and Schreiber, 2012). Seeds
580 may be blown along the ground following initial deposition, which our model does not
581 account for. The classic WALD dispersal model employed here assumes uniform grass
582 cover, with seeds trapped below the height of this grass canopy. As in aridlands world-
583 wide, our northern Chihuahuan Desert study region is characterized by a high percentage
584 of bare ground, especially in areas of high creosote density (Fig. 1). New approaches are
585 needed to extend mechanistic dispersal modeling to accommodate this feature of arid-
586 lands, as others have recognized (Thompson et al., 2014). The potential roles for both
587 biotic and abiotic secondary dispersal vectors makes our dispersal kernel a conservative
588 estimate of seed movement.

589 Our model focused on intra-specific density dependence but inter-specific plant-plant
590 interactions may be an important element of shrub encroachment. For example, over-
591 grazing is a hypothesized driver of shrub encroachment due to release from grass com-
592 petition and reduction of grassland fires (Van Auken, 2000). Our shrub encroachment
593 model considered only one “side” of the grass-shrub ecotone, assuming that the shrub
594 population spreads into empty space. Explicit consideration of grass competition or fa-
595 cilitation may enrich our understanding of shrub expansion or lack thereof in this and

596 other systems. However, our transplant experiment provided no strong evidence for an
597 influence of grass cover on seedling survival (Appendix B). Similarly, grass competition
598 had no effect on germination and survival of mesquite (*Prosopis glandulosa*) shrubs in Chi-
599 huahuan Desert grassland (Weber-Grullon et al., 2022). While our current data do not
600 allow us to quantify whether and how strongly resident grasses may slow down shrub
601 encroachment, we can infer that competitive effects of grasses on shrubs are weaker than
602 competitive effects of shrubs on shrubs (since shrub fitness increased from high to low
603 shrub density). Therefore our conclusion that the encroachment wave is pulled implicitly
604 accounts for any effects of grass cover.

605 While our data reveal strong negative density dependence, we know little about the
606 underlying mechanisms that give rise to this pattern. What is it about high shrub density
607 environments that suppress survival and reproduction? The abundance of bare ground
608 in core shrubland suggests that shrubs do not compete for space. However, Brisson
609 and Reynolds (1994) found strong competition for space belowground, with crowded
610 neighborhoods constraining root systems. Also, root development of creosote seedlings
611 can respond rapidly to the availability of soil moisture (Obrist and Arnone Iii, 2003),
612 suggesting that competition for water may be another element of density dependence.
613 Finally, negative density dependence in plants may also be mediated by consumers or
614 soil microbes. Better understanding the environmental drivers of density dependence
615 will enable better prediction for how the encroachment wave may respond to future
616 environmental change.

617 *Conclusions..* Understanding and predicting the dynamics of woody-herbaceous eco-
618 tones requires that we build knowledge of the fates of the rare individuals that disperse
619 from core habitat and cross habitat boundaries. For a creosote bush, there is no better
620 place to be than alone in a grassland, and that key result governs the spatial dynamics of

621 this population. we found that wave of creosote bush expansion into Chihuahuan desert
622 grassland is pulled by peak fitness at the leading edge. However, it is pulled so slowly
623 that it is effectively stalled, a model-derived prediction that is supported by independent
624 data. Acute sensitivity to seedling recruitment and survival leaves this system poised for
625 pulses of expansion under the right conditions; what exactly those conditions is not yet
626 fully resolved.

627 Theory tells us that the occurrence and pace of population expansion are driven by
628 the combined influence of dispersal and density-dependent demography. We suggest
629 that the concepts and tools of spatial population biology may facilitate advances in the
630 study and management of woody plant encroachment, a globally relevant phenomenon
631 which, like all spreading populations, must be driven by birth, death, and movement.

632 **Acknowledgements**

633 **Author contributions**

634 **Data accessibility**

635 **Literature Cited**

636 Allen, A., W. Pockman, C. Restrepo, and B. Milne. 2008. Allometry, growth and pop-
637 ulation regulation of the desert shrub *Larrea tridentata*. *Functional Ecology* pages
638 197–204.

639 Bowers, J. E., R. M. Turner, and T. L. Burgess. 2004. Temporal and spatial patterns in
640 emergence and early survival of perennial plants in the Sonoran Desert. *Plant Ecology*
641 **172**:107–119.

- 642 Boyd, R. S., and G. D. Brum. 1983. Postdispersal reproductive biology of a Mojave Desert
643 population of *Larrea tridentata* (Zygophyllaceae). *American Midland Naturalist* pages
644 25–36.
- 645 Brandt, J. S., M. A. Haynes, T. Kuemmerle, D. M. Waller, and V. C. Radeloff. 2013.
646 Regime shift on the roof of the world: Alpine meadows converting to shrublands in
647 the southern Himalayas. *Biological Conservation* **158**:116–127.
- 648 Brisson, J., and J. F. Reynolds. 1994. The effect of neighbors on root distribution in a
649 creosotebush (*Larrea tridentata*) population. *Ecology* **75**:1693–1702.
- 650 Buffington, L. C., and C. H. Herbel. 1965. Vegetational changes on a semidesert grassland
651 range from 1858 to 1963. *Ecological monographs* **35**:139–164.
- 652 Bullock, J. M., S. M. White, C. Prudhomme, C. Tansey, R. Perea, and D. A. Hooftman.
653 2012. Modelling spread of British wind-dispersed plants under future wind speeds in
654 a changing climate. *Journal of Ecology* **100**:104–115.
- 655 Cabral, A., J. De Miguel, A. Rescia, M. Schmitz, and F. Pineda. 2003. Shrub encroachment
656 in Argentinean savannas. *Journal of Vegetation Science* **14**:145–152.
- 657 Collins, S. L., J. B. Nippert, J. M. Blair, J. M. Briggs, P. Blackmore, and Z. Ratajczak.
658 2021. Fire frequency, state change and hysteresis in tallgrass prairie. *Ecology Letters*
659 **24**:636–647.
- 660 D’Odorico, P., J. D. Fuentes, W. T. Pockman, S. L. Collins, Y. He, J. S. Medeiros,
661 S. DeWekker, and M. E. Litvak. 2010. Positive feedback between microclimate and
662 shrub encroachment in the northern Chihuahuan desert. *Ecosphere* **1**:1–11.
- 663 D’odorico, P., Y. He, S. Collins, S. F. De Wekker, V. Engel, and J. D. Fuentes. 2013.

664 Vegetation–microclimate feedbacks in woodland–grassland ecotones. *Global Ecology*
665 and *Biogeography* **22**:364–379.

666 D’Odorico, P., G. S. Okin, and B. T. Bestelmeyer. 2012. A synthetic review of feedbacks
667 and drivers of shrub encroachment in arid grasslands. *Ecohydrology* **5**:520–530.

668 Ellner, S. P., D. Z. Childs, M. Rees, et al. 2016. Data-driven modelling of structured
669 populations. *A practical guide to the Integral Projection Model*. Cham: Springer .

670 Ellner, S. P., and S. J. Schreiber. 2012. Temporally variable dispersal and demography can
671 accelerate the spread of invading species. *Theoretical Population Biology* **82**:283–298.

672 Gandhi, S. R., E. A. Yurtsev, K. S. Korolev, and J. Gore. 2016. Range expansions transition
673 from pulled to pushed waves as growth becomes more cooperative in an experimental
674 microbial population. *Proceedings of the National Academy of Sciences* **113**:6922–6927.

675 Gardner, J. L. 1951. Vegetation of the creosotebush area of the Rio Grande Valley in New
676 Mexico. *Ecological Monographs* **21**:379–403.

677 Gibbens, R., R. McNeely, K. Havstad, R. Beck, and B. Nolen. 2005. Vegetation changes in
678 the Jornada Basin from 1858 to 1998. *Journal of Arid Environments* **61**:651–668.

679 Goslee, S., K. Havstad, D. Peters, A. Rango, and W. Schlesinger. 2003. High-resolution
680 images reveal rate and pattern of shrub encroachment over six decades in New Mexico,
681 USA. *Journal of Arid Environments* **54**:755–767.

682 Grover, H. D., and H. B. Musick. 1990. Shrubland encroachment in southern New Mex-
683 ico, USA: an analysis of desertification processes in the American Southwest. *Climatic*
684 *change* **17**:305–330.

685 Harrington, G. N. 1991. Effects of soil moisture on shrub seedling survival in semi-arid
686 grassland. *Ecology* **72**:1138–1149.

687 Hsieh, C.-I., and G. G. Katul. 1997. Dissipation methods, Taylor’s hypothesis, and
688 stability correction functions in the atmospheric surface layer. *Journal of Geophysical*
689 *Research: Atmospheres* **102**:16391–16405.

690 Huang, H., L. D. Anderegg, T. E. Dawson, S. Mote, and P. D’Odorico. 2020. Critical tran-
691 sition to woody plant dominance through microclimate feedbacks in North American
692 coastal ecosystems. *Ecology* **101**:e03107.

693 Jongejans, E., K. Shea, O. Skarpaas, D. Kelly, and S. P. Ellner. 2011. Importance of
694 individual and environmental variation for invasive species spread: a spatial integral
695 projection model. *Ecology* **92**:86–97.

696 Katul, G., A. Porporato, R. Nathan, M. Siqueira, M. Soons, D. Poggi, H. Horn, and S. A.
697 Levin. 2005. Mechanistic analytical models for long-distance seed dispersal by wind.
698 *The American Naturalist* **166**:368–381.

699 Keitt, T. H., M. A. Lewis, and R. D. Holt. 2001. Allee effects, invasion pinning, and
700 species’ borders. *The American Naturalist* **157**:203–216.

701 Kelleway, J. J., K. Cavanaugh, K. Rogers, I. C. Feller, E. Ens, C. Doughty, and N. Saintilan.
702 2017. Review of the ecosystem service implications of mangrove encroachment into
703 salt marshes. *Global Change Biology* **23**:3967–3983.

704 Knapp, A. K., J. M. Briggs, S. L. Collins, S. R. Archer, M. S. BRET-HARTE, B. E. Ewers,
705 D. P. Peters, D. R. Young, G. R. Shaver, E. Pendall, et al. 2008. Shrub encroachment in
706 North American grasslands: shifts in growth form dominance rapidly alters control of
707 ecosystem carbon inputs. *Global Change Biology* **14**:615–623.

- 708 Kot, M., M. A. Lewis, and P. van den Driessche. 1996. Dispersal data and the spread of
709 invading organisms. *Ecology* **77**:2027–2042.
- 710 Lewis, M., and P. Kareiva. 1993. Allee dynamics and the spread of invading organisms.
711 *Theoretical Population Biology* **43**:141–158.
- 712 Lewis, M. A., M. G. Neubert, H. Caswell, J. S. Clark, and K. Shea, 2006. A guide to cal-
713 culating discrete-time invasion rates from data. Pages 169–192 *in* *Conceptual ecology*
714 *and invasion biology: reciprocal approaches to nature*. Springer.
- 715 Mabry, T. J., J. H. Hunziker, D. Difeo Jr, et al. 1978. Creosote bush: biology and chemistry
716 of *Larrea* in New World deserts. Dowden, Hutchinson & Ross, Inc.
- 717 Maddox, J. C., and S. Carlquist. 1985. Wind dispersal in Californian desert plants:
718 experimental studies and conceptual considerations. *Aliso: A Journal of Systematic*
719 *and Evolutionary Botany* **11**:77–96.
- 720 Moore, D., and K. Hall, 2022. Meteorology Data from the Sevilleta Na-
721 tional Wildlife Refuge, New Mexico. Environmental Data Initiative.
722 <https://doi.org/10.6073/pasta/d56307b398e28137dabaa6994f0f5f92>.
- 723 Moreno-de las Heras, M., L. Turnbull, and J. Wainwright. 2016. Seed-bank structure
724 and plant-recruitment conditions regulate the dynamics of a grassland-shrubland Chi-
725 huahuan ecotone. *Ecology* **97**:2303–2318.
- 726 Mugasi, S., E. Sabiiti, and B. Tayebwa. 2000. The economic implications of bush en-
727 croachment on livestock farming in rangelands of Uganda. *African Journal of Range*
728 *and Forage Science* **17**:64–69.
- 729 Nathan, R., G. G. Katul, G. Bohrer, A. Kuparinen, M. B. Soons, S. E. Thompson, A. Trakht-

- 730 enbrot, and H. S. Horn. 2011. Mechanistic models of seed dispersal by wind. Theoret-
731 ical Ecology **4**:113–132.
- 732 Neubert, M. G., and H. Caswell. 2000. Demography and dispersal: calculation and
733 sensitivity analysis of invasion speed for structured populations. Ecology **81**:1613–
734 1628.
- 735 Oba, G., E. Post, P. Syvertsen, and N. Stenseth. 2000. Bush cover and range condition
736 assessments in relation to landscape and grazing in southern Ethiopia. Landscape
737 ecology **15**:535–546.
- 738 Obrist, D., and J. Arnone Iii. 2003. Increasing CO₂ accelerates root growth and enhances
739 water acquisition during early stages of development in *Larrea tridentata*. New Phy-
740 tologist **159**:175–184.
- 741 Pan, S., and G. Lin. 2012. Invasion traveling wave solutions of a competitive system with
742 dispersal. Boundary Value Problems **2012**:120.
- 743 Parizek, B., C. M. Rostagno, and R. Sottini. 2002. Soil erosion as affected by shrub
744 encroachment in northeastern Patagonia. Rangeland Ecology & Management/Journal
745 of Range Management Archives **55**:43–48.
- 746 Peters, D. P., and J. Yao. 2012. Long-term experimental loss of foundation species:
747 consequences for dynamics at ecotones across heterogeneous landscapes. Ecosphere
748 **3**:1–23.
- 749 Petrie, M., S. Collins, D. Gutzler, and D. Moore. 2014. Regional trends and local vari-
750 ability in monsoon precipitation in the northern Chihuahuan Desert, USA. Journal of
751 Arid Environments **103**:63–70.

- 752 Ratajczak, Z., J. B. Nippert, and S. L. Collins. 2012. Woody encroachment decreases
753 diversity across North American grasslands and savannas. *Ecology* **93**:697–703.
- 754 Ratajczak, Z., J. B. Nippert, J. C. Hartman, and T. W. Ocheltree. 2011. Positive feedbacks
755 amplify rates of woody encroachment in mesic tallgrass prairie. *Ecosphere* **2**:1–14.
- 756 Raupach, M. 1994. Simplified expressions for vegetation roughness length and zero-
757 plane displacement as functions of canopy height and area index. *Boundary-Layer*
758 *Meteorology* **71**:211–216.
- 759 Ravi, S., P. D’Odorico, S. L. Collins, and T. E. Huxman. 2009. Can biological invasions
760 induce desertification? *The New Phytologist* **181**:512–515.
- 761 Reed, M., L. Stringer, A. Dougill, J. Perkins, J. Atlhopheng, K. Mulale, and N. Favretto.
762 2015. Reorienting land degradation towards sustainable land management: Linking
763 sustainable livelihoods with ecosystem services in rangeland systems. *Journal of envi-*
764 *ronmental management* **151**:472–485.
- 765 Reynolds, J. F., R. A. Virginia, P. R. Kemp, A. G. De Soyza, and D. C. Tremmel. 1999.
766 Impact of drought on desert shrubs: effects of seasonality and degree of resource
767 island development. *Ecological Monographs* **69**:69–106.
- 768 Rogers, H. S., N. G. Beckman, F. Hartig, J. S. Johnson, G. Pufal, K. Shea, D. Zurell, J. M.
769 Bullock, R. S. Cantrell, B. Loiselle, et al. 2019. The total dispersal kernel: a review and
770 future directions. *AoB Plants* **11**:plz042.
- 771 Roques, K., T. O’connor, and A. R. Watkinson. 2001. Dynamics of shrub encroachment in
772 an African savanna: relative influences of fire, herbivory, rainfall and density depen-
773 dence. *Journal of Applied Ecology* **38**:268–280.

- 774 Schlesinger, W. H., and A. M. Pilmanis. 1998. Plant-soil interactions in deserts. Biogeo-
775 chemistry **42**:169–187.
- 776 Schlesinger, W. H., J. A. Raikes, A. E. Hartley, and A. F. Cross. 1996. On the spatial
777 pattern of soil nutrients in desert ecosystems: ecological archives E077-002. Ecology
778 **77**:364–374.
- 779 Schlesinger, W. H., J. F. Reynolds, G. L. Cunningham, L. F. Huenneke, W. M. Jarrell, R. A.
780 Virginia, and W. G. Whitford. 1990. Biological feedbacks in global desertification.
781 Science **247**:1043–1048.
- 782 Sirami, C., and A. Monadjem. 2012. Changes in bird communities in Swaziland savannas
783 between 1998 and 2008 owing to shrub encroachment. Diversity and Distributions
784 **18**:390–400.
- 785 Skarpaas, O., and K. Shea. 2007. Dispersal patterns, dispersal mechanisms, and invasion
786 wave speeds for invasive thistles. The American Naturalist **170**:421–430.
- 787 Stephens, P. A., W. J. Sutherland, and R. P. Freckleton. 1999. What is the Allee effect?
788 Oikos pages 185–190.
- 789 Sullivan, L. L., B. Li, T. E. Miller, M. G. Neubert, and A. K. Shaw. 2017. Density depen-
790 dence in demography and dispersal generates fluctuating invasion speeds. Proceed-
791 ings of the National Academy of Sciences **114**:5053–5058.
- 792 Taylor, C. M., and A. Hastings. 2005. Allee effects in biological invasions. Ecology Letters
793 **8**:895–908.
- 794 Thompson, S. E., S. Assouline, L. Chen, A. Trahktenbrot, T. Svoray, and G. G. Katul. 2014.
795 Secondary dispersal driven by overland flow in drylands: Review and mechanistic
796 model development. Movement ecology **2**:7.

- 797 Trollope, W., F. Hobson, J. Danckwerts, and J. Van Niekerk. 1989. Encroachment and
798 control of undesirable plants. *Veld management in the Eastern Cape* pages 73–89.
- 799 Turnbull, L., J. Wainwright, and R. E. Brazier. 2010. Changes in hydrology and erosion
800 over a transition from grassland to shrubland. *Hydrological Processes: An Interna-*
801 *tional Journal* **24**:393–414.
- 802 Van Auken, O. 2009. Causes and consequences of woody plant encroachment into
803 western North American grasslands. *Journal of environmental management* **90**:2931–
804 2942.
- 805 Van Auken, O. W. 2000. Shrub invasions of North American semiarid grasslands. *Annual*
806 *review of ecology and systematics* **31**:197–215.
- 807 Vasek, F. C. 1980. Creosote bush: Long-lived clones in the Mojave Desert. *American*
808 *Journal of Botany* **67**:246–255.
- 809 Veit, R. R., and M. A. Lewis. 1996. Dispersal, population growth, and the Allee effect: dy-
810 namics of the house finch invasion of eastern North America. *The American Naturalist*
811 **148**:255–274.
- 812 Wang, M.-H., M. Kot, and M. G. Neubert. 2002. Integro-difference equations, Allee effects,
813 and invasions. *Journal of mathematical biology* **44**:150–168.
- 814 Weber-Grullon, L., L. Gherardi, W. A. Rutherford, S. R. Archer, and O. E. Sala. 2022.
815 Woody-plant encroachment: Precipitation, herbivory, and grass-competition interact
816 to affect shrub recruitment. *Ecological Applications* **32**:e2536.
- 817 Wiernga, J. 1993. Representative roughness parameters for homogeneous terrain.
818 *Boundary-Layer Meteorology* **63**:323–363.

- 819 Wilcox, B. P., A. Birt, S. D. Fuhlendorf, and S. R. Archer. 2018. Emerging frameworks for
820 understanding and mitigating woody plant encroachment in grassy biomes. *Current*
821 *Opinion in Environmental Sustainability* **32**:46–52.
- 822 Williams, J. L., T. E. Miller, and S. P. Ellner. 2012. Avoiding unintentional eviction from
823 integral projection models. *Ecology* **93**:2008–2014.
- 824 Wood, S. 2017. *Generalized Additive Models: An Introduction with R*. 2 edition. Chap-
825 man and Hall/CRC.

Appendix A: Dispersal kernel modeling

WALD dispersal kernel. In order to create the dispersal kernel, we first take the wind speeds at measurement height z_m and correct them to find wind speed U for any height H by using the logarithmic wind profile ³

$$U = \frac{1}{H} \int_{d+z_0}^H \frac{u^*}{K} \log \left(\frac{z-d}{z_0} \right) dz \quad (\text{A1})$$

given in Bullock et al. (2012) equation 6, with the notation slightly modified. Here, z is the height above the ground, K is the von Karman constant, and u^* is the friction velocity. The zero-plane displacement d and roughness length z_0 are surface roughness parameters that, for a grass canopy height h above the ground, are approximated by $d \approx 0.7h$ and $z_0 \approx 0.1h$. These estimates are from Raupach (1994) for a canopy area index $\Lambda = 1$ in which the sum of grass canopy elements is equal to the unit area being measured. A 0.15 m grass height at our study site gives $d = 0.105$ and z_0 , which are suitable approximations for grassland (Wiernga, 1993). Calculations of u^* were done using equation A2 from Skarpaas and Shea (2007), in which

$$u^* = KU_m \left[\log \left(\frac{z_m - d}{z_0} \right) \right]^{-1} \quad (\text{A2})$$

and U_m is the mean wind velocity at the measurement height z_m . Values for the turbulent flow parameter σ were then calculated using the estimate made by Skarpaas and Shea (2007) in their equation A4, where

$$\sigma = 2A_w^2 \sqrt{\frac{K(z-d)u^*}{C_0 U}} \quad (\text{A3})$$

³We need to describe and cite the wind data used here.

and C_0 is the Kolmogorov constant. A_w is a constant that relates vertical turbulence to friction velocity and is approximately equal to 1.3 under the assumptions of above-canopy flow made by Skarpaas and Shea (2007), based off calculations from Hsieh and Katul (1997). In addition, the assumption that $z = H$ was made in order to make the calculation of σ more feasible.⁴

The values from the previous three equations give us the necessary information to calculate μ' and λ' , thus allowing us to create the WALD distribution $p(r)$. However, the base WALD model does not take into account variation in wind speeds or seed terminal velocities, which limits its applicability in systems where such variation is present. In order to account for this variation, we integrate the WALD model over distributions of these two variables using the same method as Skarpaas and Shea (2007). Additionally, the WALD model assumes seed release from a single point source, which is not realistic for creosote bush; because seeds are released across the entire height of the shrub rather than from a point source, we integrated $p(r)$ across the uniform distribution from the grass canopy height to the shrub height. Thus, under the assumptions that the height at which a seed is located does not affect its probability of being released and that seeds are evenly distributed throughout the shrub, this gives the dispersal kernel $K(r)$, where

$$K(r) = \iiint p(F)p(U)p(z)p(r) dF dU dz \quad (\text{A4})$$

and $p(F)$ and $p(U)$ are the PDFs of the terminal velocity F and wind speed U , respectively, and $p(z)$ is the uniform distribution from h to H .

Dispersal data collection. The distribution $p(F)$ in the integral above was constructed using experimentally determined seed terminal velocities. This was done by using

⁴Can you describe this assumption in biological terms?

laboratory-based seed release experiments with a high-speed camera and motion tracking software to determine position as a function of time. We then used the Levenberg-Marquardt algorithm to solve a quadratic-drag equation of motion for F . Before seeds were released, they were dried, dyed with yellow fluorescent powder, and then put against a black background to improve visibility and make tracking easier. While the powder added mass to the seeds, this added mass only yielded an approximately 2.5% increase, likely having little effect on terminal velocities. Measurements were conducted for 48 seeds that were randomly chosen from a seed pool derived from different plants, and then an empirical PDF of terminal velocities was constructed using the data. Constructing $p(U)$ involved creating an empirical PDF of hourly wind speeds using data from Sevilleta LTER meteorological station 49, the station closest to our transects. We used wind speed data collected hourly from 2015 to 2019 (Moore and Hall, 2022).

Appendix B: Additional results

Pr(Survival)	df	dAIC
~size + transplant + size:transplant + (1 transect)	11.50	1.72
~size + transplant + density + size:transplant + density:transplant + (1 transect)	13.19	0.19
~size + transplant + density + size:transplant + density:transplant + size:density + size:transplant:density + (1 transect)	14.22	0.00

Table B1: AIC model selection for survival probability.

mean(size)	sd(size)	df	dAIC
~size + (1 transect)	~1	3.00	1024.88
~size + density + (1 transect)	~1	8.50	977.23
~size + density + size:density + (1 transect)	~1	10.47	975.17
~size + (1 transect)	~size	9.65	146.23
~size + density + (1 transect)	~size	16.24	19.45
~size + density + size:density + (1 transect)	~size	18.55	19.62
~size + (1 transect)	~size + density	10.40	115.52
~size + density + (1 transect)	~size + density	18.97	0.08
~size + density + size:density + (1 transect)	~size + density	21.33	0.00

Table B2: AIC model selection for mean and variance of future size

Pr(Flowering)	df	dAIC
~size + (1 transect)	5.78	0.63
~size + density + (1 transect)	6.80	2.32
~size + density + size:density + (1 transect)	7.24	0.00

Table B3: AIC model selection for flowering probability.

No. fruits	df	dAIC
~size + (1 transect)	14.25	71.99
~size + density + (1 transect)	5.52	0.00
~size + density + size:density + (1 transect)	6.23	0.37

Table B4: AIC model selection for fruit number.

Pr(Recruitment)	df	dAIC
~(1 transect)	6.57	0.00
~density + (1 transect)	7.39	0.93

Table B5: AIC model selection for recruitment probability.

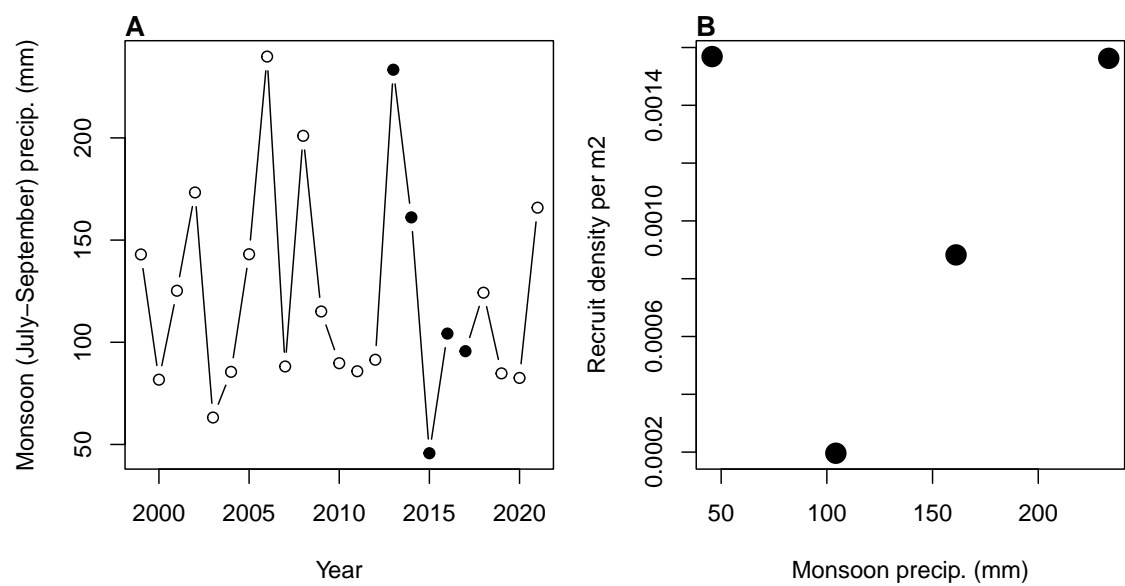


Figure B1: .

mean(size)	sd(size)	df	dAIC
~(1 transect)	~1	2.00	2.90
~density+(1 transect)	~1	4.42	0.00
~(1 transect)	~density	3.00	4.74
~density+(1 transect)	~density	5.56	1.21

Table B6: AIC model selection for mean and variance of recruit size.